

On the absence of the Chiral Magnetic Effect in equilibrium QCD

B. B. Brandt,^a G. Endrődi,^a E. Garnacho-Velasco,^a and G. Markó^a

^a*Fakultät für Physik, Universität Bielefeld,
Universitätsstraße 25, 33615 Bielefeld, Germany*

E-mail: brandt@physik.uni-bielefeld.de,
endrodi@physik.uni-bielefeld.de, egarnacho@physik.uni-bielefeld.de,
gmarko@physik.uni-bielefeld.de

ABSTRACT: In this paper we investigate the chiral magnetic effect (CME): the generation of an electric current due to a homogeneous background magnetic field and a homogeneous chiral imbalance in QCD. We demonstrate that the leading coefficient describing the CME vanishes in equilibrium, both for free fermions as well as in full QCD. Our full QCD results are based on continuum extrapolated lattice simulations using dynamical staggered quarks with physical masses as well as quenched Wilson quarks. We show that it is crucial that a gauge invariant ultraviolet regularization is used to compute the CME and elaborate on why some of the existing in-equilibrium calculations of this effect gave a nonzero result. We stress that our findings imply the absence of a time-independent CME current flowing in equilibrium QCD, but do not concern the CME as an out-of-equilibrium, time-dependent effect.

Contents

1	Introduction	1
2	The Chiral Magnetic Effect in equilibrium	2
2.1	Currents and chemical potentials	3
2.2	Analytic result for the CME conductivity for free fermions	4
2.3	Chiral imbalance	6
3	Lattice methods	7
3.1	Lattice setup – staggered quarks	8
3.2	Lattice setup – Wilson quarks	11
3.3	Simulation setup	13
4	Results	14
4.1	Free quarks	14
4.2	Quenched theory	14
4.3	QCD at physical quark masses	17
5	Summary and outlook	19
A	Parameterization dependence of the unregularized C_{CME} in the free case	20
B	CME in the free case from the two-point function at finite temperature	22
C	Axial susceptibility in the free case	23
D	CME with free staggered fermions	24

1 Introduction

The vacuum of Quantum Chromodynamics (QCD) is not empty space but a medium filled with virtual particles giving rise to the low-energy facets of the strong interactions. In particular, the topological fluctuations of the gluon fields induce some of the most fascinating aspects of the theory. In specific external environments – such as background electromagnetic fields or in rotating coordinate systems – a series of intricate transport phenomena arise, for which the quantum anomaly of QCD plays a special role. These are so-called anomalous transport effects [1–3].

The most prominent example for anomalous transport phenomena is the Chiral Magnetic Effect (CME), the generation of an electromagnetic current in the presence of a magnetic field and chiral imbalance [4, 5]. Via the CME, topological gluonic fluctuations,

converted to chirality fluctuations through the anomaly, are expected to produce observable signatures in different physical settings. The CME current has been detected in condensed matter systems [6] and is actively sought for in heavy ion collision experiments [7–9]. Moreover, the CME has been argued to play a relevant role in astrophysics and cosmology [10], e.g. for neutrino transport in supernovae [11].

The CME has been treated within a series of theoretical approaches, including QCD models and effective theories [12] (see the review [13]), holography [14–16], hydrodynamics [17, 18], kinetic theory [19] and lattice simulations [20–24], see also the lattice studies looking for indirect effects of the CME [25–30]. In this work we will focus on the theoretical aspects of this effect using both lattice and continuum regularizations of the quantum field theory. Since the very first study [31], the theoretical understanding of the CME has greatly evolved. By now the CME is understood as an out-of-equilibrium effect, for which a time-dependent electric current is induced by a time-dependent chiral imbalance. The most general argument for the absence of an in-equilibrium CME comes from Bloch’s theorem, which forbids global conserved currents to flow in equilibrium [32]. However, there are several equilibrium studies in the literature that did predict a non-vanishing CME current. In particular, this includes many of the above listed continuum calculations, based on the static Dirac eigenvalues for free fermions, as well as in-equilibrium lattice simulations [20, 21]. Given the high importance of the CME for a multitude of physical settings, these contradictory findings clearly call for clarification.

In this paper we will determine the CME conductivity in equilibrium from the first principles of QCD. In particular, we will present the first results for the conductivity based on fully interacting in-equilibrium lattice QCD simulations employing physical quark masses and a continuum extrapolation. Our approach generalizes the method that we developed in [33] for the determination of the conductivity for the chiral separation effect (CSE), an analogous anomalous transport phenomenon [34, 35]. Moreover, we will revisit the calculation of the CME current for free fermions using a gauge-invariant regularization. All our results are compatible with a vanishing CME current in equilibrium. In turn, we show how regularizations incompatible with the gauge symmetry, more generically, the use of a non-conserved electric current, can erroneously give nonzero results. We stress that our findings do not concern the out-of-equilibrium effect that arises for time-dependent external fields or chiral imbalance [5, 36].

2 The Chiral Magnetic Effect in equilibrium

We start our discussion of the CME in thermal equilibrium by describing the setup. We consider a system in the presence of a background magnetic field B , where the chiral density is nonzero. The chiral imbalance is parameterized by a chiral chemical potential μ_5 , whose detailed properties will be discussed below. The generation of a vector current J_ν (parallel to B) in this scenario is what is known as the chiral magnetic effect. We will be interested in the linear term C_{CME} in a Taylor-expansion of this current for weak B and μ_5 , which we will refer interchangeably as CME conductivity coefficient or CME conductivity. Apart

from section 2.2 and unless explicitly stated otherwise, throughout the paper we work in Euclidean space-time and with Hermitian Dirac matrices which satisfy $\{\gamma_\mu, \gamma_\nu\} = 2\delta_{\mu\nu}$.

2.1 Currents and chemical potentials

We consider the vector current coupled to the electric charge,¹

$$J_\nu = \sum_f \frac{q_f}{e} \frac{T}{V} \int d^4x \bar{\psi}_f(x) \gamma_\nu \psi_f(x), \quad (2.1)$$

where $f = u, d, s, \dots$ labels the quark flavors and q_f are the corresponding electric charges. The charge density J_4 can be controlled by a charge chemical potential in the grand canonical ensemble. Analogously, the chiral density can also be parameterized by a chiral chemical potential μ_5 , which couples to the fourth component of the associated axial current,

$$J_{\nu 5} = \sum_f \frac{T}{V} \int d^4x \bar{\psi}_f(x) \gamma_\nu \gamma_5 \psi_f(x), \quad (2.2)$$

which we normalized here so that each quark flavor contributes with unit weight.

The chiral chemical potential μ_5 is clearly not a chemical potential in the standard thermodynamic sense, since the charge it couples to is not conserved (due to the nonzero quark mass as well as the chiral anomaly). It can either be thought of as a mere parameter that controls the chiral imbalance of the system or as the constant temporal component of an axial gauge field. In any case, one could be concerned if μ_5 does really induce chiral imbalance or if its effect is washed out due to the non-conserved nature of the axial charge. Below we will demonstrate, both for free quarks and for full QCD, that μ_5 indeed induces nonzero chirality in the system.

The CME conductivity coefficient is defined via the leading-order term in the Taylor-expansion of the electric current with respect to B and μ_5 around vanishing fields,

$$\langle J_3 \rangle = C_{\text{CME}} \mu_5 e B + \mathcal{O}(\mu_5^3, B^3). \quad (2.3)$$

Here, the magnetic field is considered in units of the elementary electric charge $e > 0$, so that we may work with the renormalization group invariant combination eB .

Although full lattice QCD simulations do not suffer from a sign problem at finite μ_5 , the introduction of this parameter for staggered fermions leads to technical difficulties which will be discussed below. Instead, we consider the Taylor-expansion of the current expectation value in the chiral chemical potential, evaluated at non-zero external magnetic fields but vanishing μ_5 . This technique will also be used for the crosschecks with Wilson

¹When considering a theory with a single quark flavor, defining the vector current and the chiral chemical potential is unambiguous up to an overall normalization. For several quark flavors, like in full QCD, there are different options for coupling the current and the chiral chemical potential to e.g. quark charges or to baryon number. Different choices can in general yield different results for the conductivities, as we showed for example in our previous study of the CSE [33]. For the CME, this choice is unimportant as we will briefly discuss below in Sec. 4.3.

fermions. We note that simulations with Wilson fermions at $\mu_5 \neq 0$ are free of the difficulties present in the staggered formulation and have already been used to investigate the CME [20, 21]. Following Eq. (2.3), the first μ_5 derivative of the CME current is given by

$$\left. \frac{\partial \langle J_3 \rangle}{\partial \mu_5} \right|_{\mu_5=0} = C_{\text{CME}} eB. \quad (2.4)$$

Using the results for this derivative for a number of different magnetic fields, C_{CME} can be extracted via numerical differentiation with respect to eB . Alternatively, using the technique developed in Ref. [37], the derivative with respect to the magnetic field can be carried out analytically. This results in an expression including a three-point function, see Refs. [38, 39] which, at leading order, is a special realization of the triangle diagram in the Adler-Bell-Jackiw anomaly. This shows the tight relation between the conductivity and the anomaly.

There is an overall proportionality constant involving the quark baryon numbers, the quark charges and the number of colors $N_c = 3$, which can be factored out of the conductivity. It reads

$$C_{\text{dof}} = N_c \sum_f \left(\frac{q_f}{e} \right)^2. \quad (2.5)$$

This overall factor can always be restored, and from this point we rescale all our results by C_{dof} unless explicitly stated otherwise.

2.2 Analytic result for the CME conductivity for free fermions

The in-equilibrium effect may be studied in the free case by constructing the electric current operator using the exact Dirac eigenvalues at $B \neq 0$ and $\mu_5 \neq 0$ [5, 40]. In these works, the conductivity coefficient was found to be given by $C_{\text{CME}} = 1/(2\pi^2)$. However, there is a critical issue related to the ultraviolet regularization, which we will illustrate below.

Let us consider one colorless fermion flavor (with mass m and charge q) at zero temperature T . Instead of working directly with the Dirac eigenvalues, we proceed as in Eq. (2.4), i.e. we will evaluate the μ_5 -derivative of the vector current in a homogeneous magnetic field background, for which free fermion propagators are known exactly [41, 42]. Unlike in the rest of the text, we will carry out the calculation using the Minkowski metric. Accordingly, the Dirac matrices are the Minkowskian ones fulfilling $\{\gamma_\mu, \gamma_\nu\} = 2\eta_{\mu\nu} = 2 \text{diag}(1, -1, -1, -1)$.

The chiral chemical potential μ_5 couples to the four-volume integral of the zeroth component of the axial current, therefore the μ_5 -derivative of the third component of the vector current can be written as

$$\left. \frac{\partial \langle J_3 \rangle}{\partial \mu_5} \right|_{\mu_5=0} = \frac{T}{V} \int d^4x \int d^4y \langle \bar{\psi}(x) \gamma_3 \psi(x) \bar{\psi}(y) \gamma_0 \gamma_5 \psi(y) \rangle. \quad (2.6)$$

We regularize in the ultraviolet using the Pauli-Villars (PV) scheme, meaning that all diagrams are replicated by the regulator fields with coefficients c_s and masses m_s . The details of the regularization are text-book knowledge found e.g. in Ref. [43]. We recall here

that we need three extra fields altogether, and reserving $s = 0$ for the physical field (with physical mass m) the parameters will be

$$c_0 = c_1 = 1, \quad c_2 = c_3 = -1, \quad (2.7)$$

$$m_0^2 = m^2, \quad m_1^2 = m^2 + 2\Lambda^2, \quad m_2^2 = m_3^2 = m^2 + \Lambda^2, \quad (2.8)$$

with $\Lambda \rightarrow \infty$ to be taken at the end of the calculation.

The derivative according to Eq. (2.4) is proportional to the CME coefficient, and using Wick's theorem we can rewrite the right-hand side of Eq. (2.6) to obtain

$$C_{\text{CME}} qB = \frac{iT}{V} \sum_{s=0}^3 c_s \int d^4x \int d^4y \text{Tr} [\gamma_3 S_s(x, y) \gamma_0 \gamma_5 S_s(y, x)], \quad (2.9)$$

where the PV fields are already taken into account, and S_s is the fermion propagator for the field s in a homogeneous magnetic background. The latter reads [42]

$$S_s(x, y) = \Phi(x, y) \int \frac{d^4p}{(2\pi)^4} e^{-ip(x-y)} \tilde{S}_s(p). \quad (2.10)$$

Here

$$\Phi(x, y) = \exp [iqB(x_1 + y_1)(x_2 - y_2)/2], \quad (2.11)$$

is the Schwinger phase, and

$$\begin{aligned} \tilde{S}_s(p) = \int_0^\infty dz e^{iz(p_0^2 - m_s^2 - p_3^2) - i \frac{p_1^2 + p_2^2}{|qB|} \tan(z|qB|)} & [\not{p} + m_s + (p_1\gamma_2 - p_2\gamma_1) \tan(zqB)] \\ & \times [1 - \gamma_1\gamma_2 \tan(zqB)]. \end{aligned} \quad (2.12)$$

Carrying out the traces

$$\begin{aligned} C_{\text{CME}} qB = -4 \sum_{s=0}^3 c_s \int \frac{d^4p}{(2\pi)^4} \int_0^\infty dz_1 dz_2 e^{i(z_1+z_2)(p_0^2 - m_s^2 - p_3^2)} & (m_s^2 - p_0^2 - p_3^2) \\ e^{-i \frac{p_1^2 + p_2^2}{qB} [\tan(z_1qB) + \tan(z_2qB)]} & [\tan(z_1qB) + \tan(z_2qB)]. \end{aligned} \quad (2.13)$$

Now we Wick rotate the momentum components and the Schwinger parameters, $p_0 = ip_4, iz_1 = Z_1, iz_2 = Z_2$. The p_1 and p_2 integrals are simple Gaussians, and evaluating them factorizes the magnetic field dependence, uncovering an explicitly linear behavior in B . This allows us to cancel the qB factor on both sides, resulting in

$$C_{\text{CME}} = \frac{1}{4\pi^3} \sum_{s=0}^3 c_s \int_{-\infty}^\infty dp_3 dp_4 \int_0^\infty dZ_1 dZ_2 e^{-(Z_1+Z_2)(p_4^2 + m_s^2 + p_3^2)} (m_s^2 + p_4^2 - p_3^2). \quad (2.14)$$

Carrying out the integrals over Z_1 and Z_2 , we arrive at the final formula

$$C_{\text{CME}} = \frac{1}{4\pi^3} \sum_{s=0}^3 c_s \int_{-\infty}^\infty dp_3 dp_4 \frac{m_s^2 + p_4^2 - p_3^2}{(m_s^2 + p_4^2 + p_3^2)^2} \propto \sum_{s=0}^3 c_s = 0. \quad (2.15)$$

The integral for a single PV field is a peculiar improper integral. On dimensional grounds, its result does not depend on m_s , and hence the sum over the PV fields inevitably vanishes due to (2.8), as we indicated in (2.15). However, to obtain a specific value for just one of the PV fields, one must choose a certain parameterization of the $p_3 - p_4$ plane spanned by the two integration variables. As we show and analyze in App. A, the result of the integration depends on the parameterization, reflecting that the unregularized result is physically meaningless. The regularized result, in turn, is $C_{\text{CME}} = 0$, irrespectively of the parameterization.

This issue with regularization has already been discussed in the literature [22, 24, 44]. In App. B we show a generalization of this calculation to finite temperature, where C_{CME} is found to vanish as well.

Another way of understanding this cancellation in equilibrium is through Bloch's theorem [45]. This no-go theorem from quantum mechanics forbids conserved currents to flow in equilibrium. The theorem can be generalized to quantum field theory and applied to the CME [32]. Since the electromagnetic current is a conserved current, Bloch's theorem forbids a non-zero expectation value in equilibrium and the CME has to be absent. We also note that this argument does not apply to the chiral separation effect (CSE) [34, 35], where a non-conserved axial current is generated in a dense magnetized medium.

We emphasize here that Bloch's theorem indicates the absence of the current expectation value at any non-zero μ_5 and B . Consequently, while focusing on the leading coefficient C_{CME} , we expect all coefficients in the Taylor expansion of Eq. (2.3) to vanish identically.

2.3 Chiral imbalance

A final remark in this section concerns the relation between the chiral chemical potential and the chiral imbalance. We emphasize that the absence of CME in equilibrium is not due to the absence of chirality in the system, but it arises from a non-trivial cancellation as shown in Eq. (2.15). In fact, it can be shown that μ_5 does induce nonzero chiral density. This can be checked by calculating the axial density J_{45} of Eq. (2.2) in the presence of a (baryon) chiral chemical potential.

However, later we will check the presence of chirality using lattice simulations, and, as already mentioned, we avoid simulations at non-zero μ_5 . Instead, we consider the coefficient of the leading order term in the expansion of $\langle J_{45} \rangle$ in μ_5 . The coefficient is equivalent to the second derivative of the partition function with respect to μ_5 , i.e. the axial susceptibility

$$\chi_5^b(T) = \frac{T}{V} \left. \frac{\partial^2 \log \mathcal{Z}}{\partial \mu_5^2} \right|_{\mu_5=0}. \quad (2.16)$$

Its nonzero value at $\mu_5 = 0$ indicates that a weak chiral chemical potential induces nonzero chiral imbalance. As we show in App. C, the susceptibility is a bare observable, subject to additive renormalization, which we indicate by the superscript b . The divergent part can be removed by subtracting the contribution at $T = 0$,

$$\chi_5(T) = \chi_5^b(T) - \chi_5^b(T=0). \quad (2.17)$$

For non-interacting fermions, the renormalized axial susceptibility takes the form

$$\frac{\chi_5}{T^2} = \frac{4}{\pi^2} \int_0^\infty dp \frac{p^2}{\left(1 + e^{\sqrt{(m/T)^2 + p^2}}\right) \sqrt{(m/T)^2 + p^2}} \xrightarrow{m/T \rightarrow 0} \frac{1}{3}. \quad (2.18)$$

The calculation can again be found in App. C.

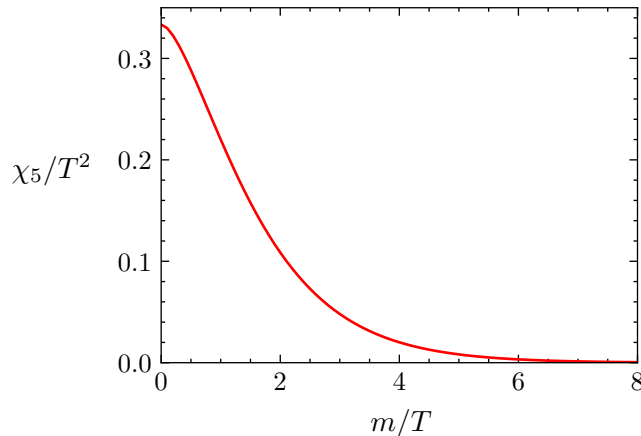


Figure 1: Analytic result (2.18) for the axial susceptibility χ_5 for non-interacting fermions as a function of m/T .

3 Lattice methods

In the following, we will use lattice simulations to check the above expectations in full QCD. In addition, our aim is to shed light on former lattice results where a non-zero C_{CME} has been observed [20, 21]. As will become clear, the reason for this apparent discrepancy with the expectations is the use of a non-conserved vector current in these studies. The appearance of a conserved current in the CME is the reason for the applicability of Bloch’s theorem to conclude that the CME should be absent in equilibrium. Retaining the conserved current in lattice simulations turns out to be vital to obtain consistent results.

We concentrate on the Euclidean lattice formulation of the chiral magnetic effect. In order to define the lattice observables required for the calculation of C_{CME} , we first need to describe how the magnetic field and the chiral chemical potential enter the discretized theory. The magnetic field B is taken to be constant and homogeneous, pointing in the third spatial direction. As already mentioned above, we will work with the renormalization group invariant combination eB .

Considering the relation between the Minkowski (indicated by the superscript M) and Euclidean Dirac matrices ($\gamma_0^{\text{M}} = \gamma_4$, $\gamma_i^{\text{M}} = i\gamma_i$), we find that the Minkowski-space observable from Eq. (2.4) is given by

$$\text{Re} \left. \frac{\partial \langle J_3 \rangle}{\partial \mu_5} \right|_{\mu_5=0}^{\text{M}} = -\text{Im} \left. \frac{\partial \langle J_3 \rangle}{\partial \mu_5} \right|_{\mu_5=0} \quad (3.1)$$

in terms of Euclidean operators. The latter will be considered in the rest of the manuscript. We also checked explicitly that the real part of the Euclidean current expectation value is consistent with zero.

3.1 Lattice setup – staggered quarks

We discuss first the setup with rooted staggered fermions, which we use to study the CME in full QCD with 2+1 flavors at the physical point. In this formalism, the partition function \mathcal{Z} can be written using the Euclidean path integral over the gluon links U

$$\mathcal{Z} = \int \mathcal{D}U \exp[-\beta S_g] \prod_f [\det M_f(U, q_f, m_f)]^{1/4}, \quad (3.2)$$

where the fermionic fields have already been integrated out to yield the fermion determinant, $\beta = 6/g^2$ denotes the inverse gauge coupling and m_f are the quark masses for each flavor $f = u, d, s$. In Eq. (3.2), S_g is the gluonic action and M_f is the massive staggered Dirac operator, which contains the quark charges $q_u/2 = -q_d = -q_s = e/3$. For S_g , we used a tree-level Symanzik action, and the Dirac operator contains twice stout-smearred links, which reduce the effect of the unphysical splitting of the masses of the different taste degrees of freedom in the staggered formulation.

The quark masses are tuned to the physical point as a function of the lattice spacing a along the line of constant physics (LCP) [46]. The chiral chemical potential (just like the quark mass) has a non-trivial multiplicative renormalization constant – and also induces divergent terms in $\log \mathcal{Z}$ as we discuss in App. C. However, unlike the mass renormalization constant Z_S^{-1} , the relevant (flavor-singlet) axial-vector renormalization constant Z_A^{-1} arises from a two-loop diagram and approaches unity perturbatively in the continuum limit [47, 48]. Thus, we expect that its use would only affect discretization errors in our lattice simulations and we do not include such a multiplicative renormalization for our observables, neither an effect of μ_5 in our LCP. We mention that such effects would in any case enter at $\mathcal{O}(\mu_5^2)$ due to charge conjugation symmetry, and therefore do not impact our observable (2.4), which contains a first derivative with respect to μ_5 at $\mu_5 = 0$. The simulations are performed on a four-dimensional lattice with N_s spatial and N_t temporal points, each site n labeled by four integers $n = \{n_1, n_2, n_3, n_4\}$. The physical spatial volume is given by $V = L^3 = (aN_s)^3$ and the temperature by $T = (aN_t)^{-1}$. Also the unitary vector in the direction ν is denoted by $\hat{\nu}$.

We note that the magnetic field is included in our setup as a classical background field, so we do not consider dynamical photons in our calculations. Analogously to the SU(3) links, the electromagnetic potential enters the Dirac operator for the quark flavor f as a parallel transporter between two lattice points $u_{f\nu} = \exp(iaq_f A_\nu)$. These U(1) links are chosen such that they represent a homogeneous magnetic field in the x_3 direction. The periodic boundary conditions in our finite volume imply that the flux of the field is quantized as $eB = 6\pi N_b / (aN_s)^2$ with the integer flux quantum $N_b \in \mathbb{Z}$ [49].

The staggered transformation partially diagonalizes the Dirac operator, by mixing coordinate and Dirac indices, so that the quark fields ψ_f are transformed to the so-called

staggered fields χ_f . It is possible to find a conserved vector current and an anomalous (flavor-singlet) axial current in the staggered formalism, via the point-split bilinears [50],

$$J_\nu^f(n) = \bar{\chi}_f(n)\Gamma_\nu^f(n, m)\chi_f(m), \quad J_{\nu 5}^f(n) = \bar{\chi}_f(n)\Gamma_{\nu 5}^f(n, m)\chi_f(m), \quad (3.3)$$

involving the staggered counterparts of the Dirac matrices [51],

$$\begin{aligned} \Gamma_\nu^f(n, m) &= \frac{\eta_\nu(n)}{2} \left[U_\nu(n)u_{f\nu}(n) e^{h(\mu_5)}\delta_{n+\hat{\nu}, m} + U_\nu^\dagger(n-\hat{\nu})u_{f\nu}^*(n-\hat{\nu}) e^{-h(\mu_5)}\delta_{n-\hat{\nu}, m} \right], \\ \Gamma_{\nu 5}^f &= \frac{1}{3!} \sum_{\rho, \alpha, \beta} \epsilon_{\nu\rho\alpha\beta} \Gamma_\rho^f \Gamma_\alpha^f \Gamma_\beta^f. \end{aligned} \quad (3.4)$$

The Γ_ν^f objects also enter the staggered equivalent of the fifth Dirac matrix,

$$\Gamma_5^f = \frac{1}{4!} \sum_{\nu, \rho, \alpha, \beta} \epsilon_{\nu\rho\alpha\beta} \Gamma_\nu^f \Gamma_\rho^f \Gamma_\alpha^f \Gamma_\beta^f. \quad (3.5)$$

Above, $\eta_\nu(n) = (-1)^{\sum_{\rho < \nu} n_\rho}$ are the staggered phases and $\epsilon_{\nu\rho\alpha\beta}$ the totally antisymmetric four-index tensor with the convention $\epsilon_{1234} = +1$. These Dirac structures depend explicitly on the chiral chemical potential via the factor $e^{\pm h(\mu_5)}$. The exponential way of introducing the chiral chemical potential is analogous to the case of a baryonic one [52], which ensures the correct continuum properties of the corresponding currents. To linear order in μ_5 , the functional form can be found by noting that

$$\left. \frac{\partial M^f}{\partial \mu_5} \right|_{\mu_5=0} = \Gamma_{45}^f, \quad (3.6)$$

leading to

$$h(\mu_5) = a\mu_5 \Sigma_\nu^f(\mu_5), \quad (3.7)$$

with the staggered representations of the spin operator,

$$\Sigma_\nu^f(\mu_5) = \frac{1}{3!} \epsilon_{\nu\rho\alpha 4} \Gamma_\rho^f \Gamma_\alpha^f(\mu_5). \quad (3.8)$$

Altogether, the Dirac operator in the presence of a chiral chemical potential in the staggered formalism can be written as (notice that $\Sigma_4^f = 0$),

$$\begin{aligned} \mathcal{D}^f(n, m) &= \frac{1}{2a} \sum_{\nu=1}^4 \eta_\nu(n) \left[U_\nu(n)u_{f\nu}(n) e^{a\mu_5 \Sigma_\nu^f(\mu_5)} \delta_{m, n+\hat{\nu}} \right. \\ &\quad \left. - U_\nu^\dagger(n-\hat{\nu})u_{f\nu}^*(n-\hat{\nu}) e^{-a\mu_5 \Sigma_\nu^f(\mu_5)} \delta_{m, n-\hat{\nu}} \right]. \end{aligned} \quad (3.9)$$

Here we note the difficulties of simulating at non-zero μ_5 with staggered fermions. The Dirac operator (3.9) has a recursive dependence on μ_5 , since each spatial hopping involves the Σ_i^f operator, which itself contains spatial hoppings. Even if this dependence is truncated at a certain order, the Dirac operator becomes a highly non-local operator involving the exponentials of the Σ_i^f matrices. An alternative approach is to introduce the chiral chemical

potential in a linear way, see [53–55]. Both formulations lead to the same expressions for first derivatives like the CME current (2.4), however they differ for higher derivatives like the axial susceptibility (2.16). We get back to the latter point below in Sec. 4.3.

With these definitions, we can now perform the Grassmann integral over the staggered fields, giving the expectation value for the (volume-averaged) vector current,

$$\langle J_3 \rangle = \frac{T}{V} \frac{1}{4} \sum_f \frac{q_f}{e} \left\langle \text{Tr} \left(\Gamma_3^f M_f^{-1} \right) \right\rangle, \quad (3.10)$$

where Tr refers to a trace in color space and a summation over the lattice coordinates. The factor $1/4$ results from rooting. Now we can calculate the derivative (2.4), required to extract C_{CME} . The obtained observable is very similar to the one used to calculate the CSE conductivity [33]. It contains the usual disconnected and connected terms, together with an additional tadpole term arising due to the derivative of Γ_3^f with respect to μ_5 ,

$$\begin{aligned} C_{\text{CME}} eB = \left. \frac{\partial \langle J_3 \rangle}{\partial \mu_5} \right|_{\mu_5=0} &= \frac{T}{V} \left[\frac{1}{16} \sum_{f,f'} \frac{q_f}{e} \left\langle \text{Tr} \left(\Gamma_{45}^{f'} M_{f'}^{-1} \right) \text{Tr} \left(\Gamma_3^f M_f^{-1} \right) \right\rangle \right. \\ &\quad - \frac{1}{4} \sum_f \frac{q_f}{e} \left\langle \text{Tr} \left(\Gamma_{45}^f M_f^{-1} \Gamma_3^f M_f^{-1} \right) \right\rangle \\ &\quad \left. + \frac{1}{4} \sum_f \frac{q_f}{e} \left\langle \text{Tr} \left(\frac{\partial \Gamma_3^f}{\partial \mu_5} M_f^{-1} \right) \right\rangle \right]. \end{aligned} \quad (3.11)$$

These expectation values are to be evaluated at $\mu_5 = 0$ but nonzero magnetic field eB .

One of our most important goals is to compare with the non-vanishing CME results with Wilson fermions [20, 21], both in full QCD and in the quenched approximation. To enable a direct comparison, we also consider QCD in the quenched approximation. This approximation corresponds to dropping the fermion determinant from the partition function (3.2), while leaving the fermionic operators in the observables unchanged. This results in a non-unitary theory where quarks behave differently in operators as in loop diagrams. It is a commonly employed approximation that simplifies simulation algorithms significantly, although is only exact for infinite quark masses. For completeness, in the quenched case we employ both the staggered and the Wilson discretization of fermions.

Finally, we also calculate C_{CME} in the absence of gluonic interactions, both for Wilson and for staggered quarks. To this end, we calculated the eigenvalues and eigenvectors of the staggered Dirac operator exactly and constructed the necessary traces from these (see App. D), while for Wilson fermions we relied on stochastic techniques to estimate the traces.

Above we also introduced the axial susceptibility χ_5 , which measures the linear response of the chiral density to the introduction of μ_5 . It is an important cross-check that χ_5 is non-zero in our system, since the absence of chirality would automatically imply a

vanishing CME. In the staggered formulation, this observable reads

$$\begin{aligned} \frac{\chi_5}{T^2} = \frac{1}{TV} & \left[\frac{1}{16} \sum_{f,f'} \left\langle \text{Tr} \left(\Gamma_{45}^f M_f^{-1} \right) \text{Tr} \left(\Gamma_{45}^{f'} M_{f'}^{-1} \right) \right\rangle - \frac{1}{4} \sum_f \left\langle \text{Tr} \left(\Gamma_{45}^f M_f^{-1} \Gamma_{45}^f M_f^{-1} \right) \right\rangle \right. \\ & \left. + \frac{1}{4} \sum_f \left\langle \text{Tr} \left(\frac{\partial^2 M_f}{\partial \mu_5^2} M_f^{-1} \right) \right\rangle \right], \end{aligned} \quad (3.12)$$

where again a tadpole term is present.

3.2 Lattice setup – Wilson quarks

Next we describe our setup involving Wilson quarks. This discretization we only consider for free fermions and in the quenched approximation – simulations with dynamical non-degenerate light Wilson quarks (differing in their electric charges) would be a computationally much more challenging task.

The massive Dirac operator is

$$aM^f = C(1 - \kappa H) \quad (3.13)$$

with the hopping operator

$$\begin{aligned} H = \sum_n \sum_\nu & \left[(r - \gamma_\nu e^{a\mu_5 \delta_{\nu 4}}) U_\nu(n) u_{f\nu}(n) \delta_{n+\hat{\nu},m} \right. \\ & \left. + (r + \gamma_\nu e^{-a\mu_5 \delta_{\nu 4}}) U_\nu^\dagger(n - \hat{\nu}) u_{f\nu}^*(n - \hat{\nu}) \delta_{n-\hat{\nu},m} \right] \end{aligned}$$

and

$$C = am_f + 4, \quad \kappa = \frac{1}{2am_f + 8}. \quad (3.14)$$

The factor r is the coefficient of the usual Wilson term (taken to be unity in our setup) and κ is the hopping parameter.

We note that the chiral chemical potential does not couple to the Wilson term, since the topological part of the axial anomaly for Wilson fermions arises from terms proportional to r , and thus the anomalous axial current, to which μ_5 couples, should not contain these terms [56]. In other words, this is the equivalent of (3.6) for Wilson fermions.

In this formulation, the currents are constructed from the bispinor fields ψ_f ,

$$J_\nu^f(n) = \bar{\psi}_f(n) \Gamma_\nu^f(n, m) \psi_f(m), \quad J_{\nu 5}^f(n) = \bar{\psi}_f(n) \Gamma_{\nu 5}^f(n, m) \psi_f(m). \quad (3.15)$$

The conserved vector and anomalous axial currents again involve a point-splitting, just as for staggered quarks [56]

$$\begin{aligned} \Gamma_\nu^f(n, m) = \frac{1}{2} & \left[(\gamma_\nu e^{a\mu_5 \delta_{\nu 4}} - r) U_\nu(n) u_{f\nu}(n) \delta_{m, n+\hat{\nu}} \right. \\ & \left. + (\gamma_\nu e^{-a\mu_5 \delta_{\nu 4}} + r) U_\nu^\dagger(n - \hat{\nu}) u_{f\nu}^*(n - \hat{\nu}) \delta_{m, n-\hat{\nu}} \right], \\ \Gamma_{\nu 5}^f(n, m) = \frac{1}{2} & \left[\gamma_\nu \gamma_5 U_\nu(n) u_{f\nu}(n) e^{a\mu_5 \delta_{\nu 4}} \delta_{m, n+\hat{\nu}} \right. \\ & \left. + \gamma_\nu \gamma_5 U_\nu^\dagger(n - \hat{\nu}) u_{f\nu}^*(n - \hat{\nu}) e^{-a\mu_5 \delta_{\nu 4}} \delta_{m, n-\hat{\nu}} \right]. \end{aligned}$$

Using the above definitions, the expectation value of the vector current reads,

$$\langle J_3 \rangle = \frac{T}{V} \sum_f \frac{q_f}{e} \langle \text{Tr} \left(\Gamma_3^f M_f^{-1} \right) \rangle. \quad (3.16)$$

In this formalism, Γ_3^f only involves hoppings in the third direction, and therefore it is independent of μ_5 . Thus, the tadpole term is absent and our observable takes a simpler form than in the staggered case,

$$C_{\text{CME}} eB = \left. \frac{\partial \langle J_3 \rangle}{\partial \mu_5} \right|_{\mu_5=0} = \frac{T}{V} \left[\sum_{f,f'} \frac{q_f}{e} \langle \text{Tr} \left(\Gamma_{45}^{f'} M_{f'}^{-1} \right) \text{Tr} \left(\Gamma_3^f M_f^{-1} \right) \rangle - \sum_f \frac{q_f}{e} \langle \text{Tr} \left(\Gamma_{45}^f M_f^{-1} \Gamma_3^f M_f^{-1} \right) \rangle \right], \quad (3.17)$$

involving only disconnected and connected terms.

It is also possible to consider a local vector current

$$J_\nu^{f,\text{loc}}(n) = \bar{\psi}_f(n) \gamma_\nu \psi_f(n) \quad (3.18)$$

instead. Even though it is not conserved, it has the same quantum numbers as J_ν^f and is often employed in Wilson fermion simulations, for example for the study of various aspects of hadron physics and, what is more relevant for this work, it was also used to study the CME in quenched and dynamical QCD [20, 21]. We can introduce a chiral chemical potential μ_5^{loc} that couples to these local currents in the action. The analogue of (3.17) now reads

$$C_{\text{CME}}^{\text{loc}} eB = \left. \frac{\partial \langle J_3^{\text{loc}} \rangle}{\partial \mu_5} \right|_{\mu_5=0} = \frac{T}{V} \left[\sum_{f,f'} \frac{q_f}{e} \langle \text{Tr} \left(\Gamma_{45}^{f'} M_{f'}^{-1} \right) \text{Tr} \left(\gamma_3 M_f^{-1} \right) \rangle - \sum_f \frac{q_f}{e} \langle \text{Tr} \left(\Gamma_{45}^f M_f^{-1} \gamma_3 M_f^{-1} \right) \rangle \right]. \quad (3.19)$$

This introduction of a chemical potential is a naive extension of the continuum formulation to the discretized theory and it is well known that this leads to new ultraviolet divergences [52]. Therefore we use this setup with the non-conserved, local current merely for comparison, and we will test the impact of these ultraviolet divergences on the observable (3.19) below.

The axial susceptibility in this case takes the form

$$\chi_5 = \frac{T}{V} \left[\sum_{f,f'} \langle \text{Tr} \left(\Gamma_{45}^f M_f^{-1} \right) \text{Tr} \left(\Gamma_{45}^{f'} M_{f'}^{-1} \right) \rangle - \sum_f \langle \text{Tr} \left(\Gamma_{45}^f M_f^{-1} \Gamma_{45}^f M_f^{-1} \right) \rangle + \sum_f \left\langle \text{Tr} \left(\frac{\partial^2 M_f}{\partial \mu_5^2} M_f^{-1} \right) \right\rangle \right], \quad (3.20)$$

where now a tadpole term appears also in the Wilson formulation, since Γ_{45}^f depends on μ_5 .

3.3 Simulation setup

For our numerical calculations, we follow the same approach as in [33]. The traces are estimated with 100 Gaussian noise vectors, except for free staggered fermions where we used the exact eigensystem instead.

C_{CME} is extracted by calculating the current derivative at different values of eB , and then performing a linear fit with no constant term, via a usual χ^2 minimization method. The slope of the fitted linear function then corresponds to the CME conductivity. For the estimation of statistical uncertainties, both of the simulation points and the fits, we use the jackknife method with 10 bins. A systematic error for the coefficient is also estimated by repeating the fit successively, eliminating the data point at the largest magnetic field in each iteration, until only one point is left. The maximum difference in the slope between the original fit and the repeated fits we consider to be the systematical error of C_{CME} .

For the quenched data, we use a slightly different approach. Since the determinant is taken to be constant, the measurements at different magnetic fields are all performed on the same gauge configurations, and are therefore correlated. To take this into account, we perform correlated fits considering the covariance matrix of the data in the χ^2 minimization method. While the statistical error of these fits is again calculated with the jackknife method, we consider a less conservative estimation of the statistical error in this case. We perform a wide variety of fits by changing the number of points considered, and including fits with a cubic term to the fitting function. We then construct a histogram weighted by the Akaike information criterion and we take the standard deviation of this distribution as the systematic error of the fit.

In Fig. 2 we display two examples of the behavior of the current derivative with eB and

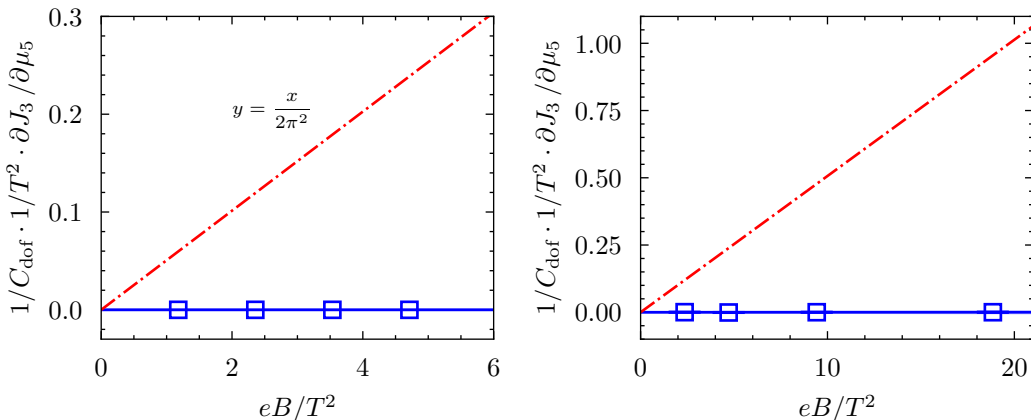


Figure 2: Derivative of the vector current with respect to the chiral chemical potential as a function of the magnetic field for a $24^3 \times 6$ lattice with staggered quarks in the free case (left) and in full QCD with $2 + 1$ flavors and physical quark masses at $T = 305$ MeV (right). The continuous line represents the optimal fit, while the band is our estimate for its uncertainty, obtained by adding the statistical and systematical errors in quadrature. The dashed-dotted line indicates a linear function with slope $1/(2\pi^2)$ for comparison.

the fits, both for free fermions and full QCD with staggered quarks. In these plots, we can see that the expected vanishing result is completely reproduced with staggered fermions. For a complete understanding of CME on the lattice with different discretizations and setups, we now present a detailed analysis of the obtained results for C_{CME} in a wide range of situations.

4 Results

4.1 Free quarks

A first simple case where we can check our setup is turning off gluonic interactions. We consider a color-singlet theory of free quarks, with mass m and charge q . In this particular case, the overall normalization factor reduces to $C_{\text{dof}} = (q/e)^2$.

In Fig. 3, we present the results for C_{CME} at three different values of m/T with staggered fermions. For the highest m/T , we also include a comparison to Wilson fermions. In each case, we show continuum extrapolations for different aspect ratios LT . Finite-size effects are only observed for small values of LT , as expected. In particular, we find $LT = 4$ to be sufficiently close to the infinite volume limit for all masses.

In this system of free fermions, we already learn what is the main conclusion of the following results: CME vanishes on a Euclidean lattice if a conserved vector current and an anomalous axial current are considered, both for staggered and Wilson fermions. For $m/T = 4$, we also show what happens when this correct setup is abandoned. For staggered quarks, excluding the tadpole terms leads to a deviation of the expected vanishing result in the continuum limit. The same happens for Wilson fermions if a local vector current is used instead of a conserved one. This is exactly the setup used in Ref. [21], whose result for the quenched theory are marked by an orange band in the bottom left plot. With this free fermion calculation we see a first indication that the reason behind the non-zero result in that work could be closely related to the use of a local vector current. This will be confirmed next, by performing QCD simulations in the quenched theory.

Before continuing with interacting theory, there is another important crosscheck that can be done. In Fig. 4, we present results for χ_5 for staggered and Wilson fermions with $m/T = 3$, where the required traces have been estimated with Gaussian random vectors in the two cases. For both discretizations, the continuum extrapolation agrees with the analytic calculation (2.18). This clearly shows that chiral density is non-zero at finite μ_5 in our setup, illustrating that the vanishing result for CME arises from a non-trivial cancellation, and not from the absence of chiral imbalance.

4.2 Quenched theory

As the next step towards the full QCD theory, we present our results in the quenched setup. This theory not only allows us to have a first look at how interactions affect the picture, but also enables a direct comparison to existing literature, in particular to the non-vanishing results in Ref. [21].

In Fig. 5, we present the calculation of C_{CME} in the quenched approximation. We use configurations generated with the plaquette gauge action at $\beta = 5.845, 5.9, 6.0, 6.25, 6.26$

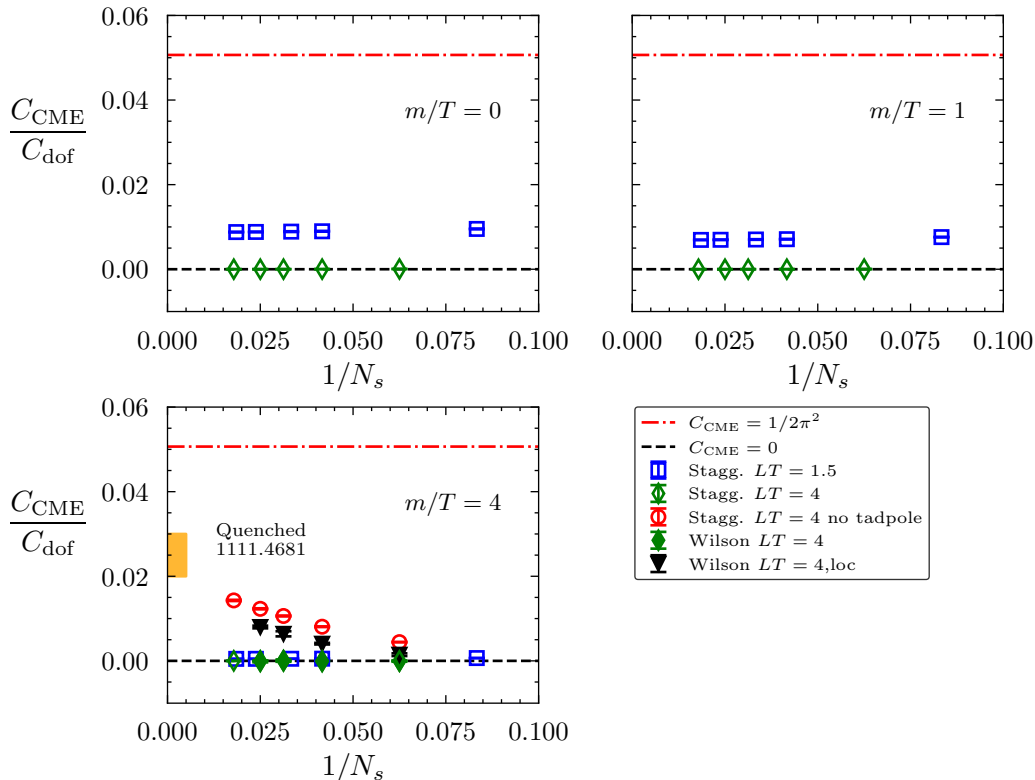


Figure 3: CME conductivity for free fermions at different values of m/T using the staggered discretization. For $m/T = 4$, Wilson fermions as well as discretizations with a non-conserved vector current are also included. The red dot-dashed line corresponds to $C_{\text{CME}} = 1/(2\pi^2)$, while the black dashed line corresponds to $C_{\text{CME}} = 0$. The quenched continuum limit estimation with Wilson fermions from Ref. [21] is depicted as an orange band for comparison.

and 6.47, and use both staggered and Wilson fermions in the valence sector. We employed these gauge configurations already in Refs. [57, 58]. The latter choice is motivated to compare to Ref. [21]. The correlator is calculated using a conserved vector current and an anomalous axial current for both discretizations, and the result clearly indicates a vanishing CME.

As mentioned above, we can compare the quenched results from [21] by simulating directly with the same parameters, but with a different approach, since the results in this work were obtained by simulating at finite chiral chemical potential and with a local vector current. In Fig. 6, we present the results for Wilson fermions in the quenched theory, with a conserved vector current and with a local one. The results with the conserved current are consistent with a vanishing C_{CME} , while the ones with the local vector current are non-zero and in agreement with the results of Ref. [21]. At this point we can conclude that the conservation of the vector current is crucial to reproduce the expected physical picture of a vanishing CME in equilibrium, and the non-zero results for C_{CME} in Ref. [21] are an

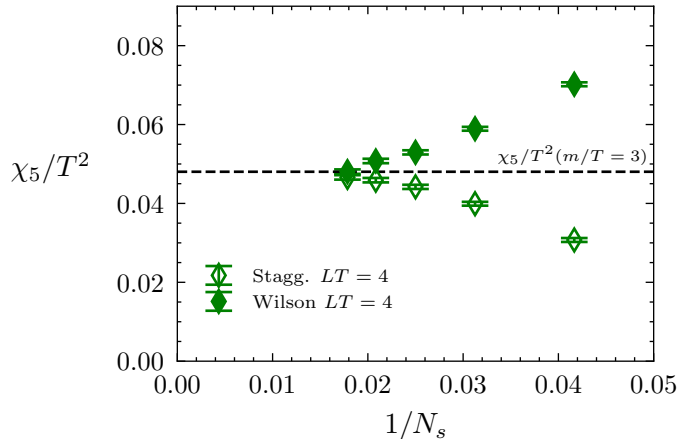


Figure 4: Axial susceptibility for free fermions with $m/T = 3$, using both the staggered and the Wilson discretizations. The black dashed line represents the value from the analytical expression (2.18) at this particular value of m/T .

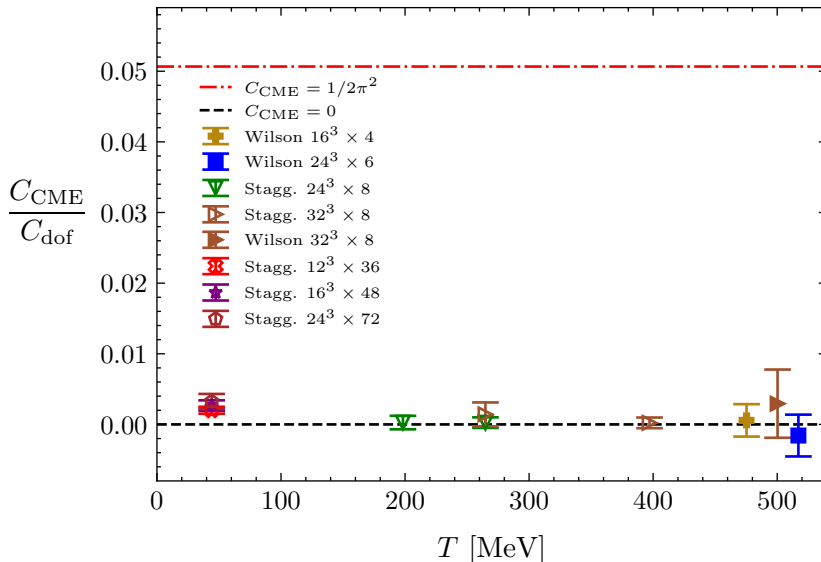


Figure 5: Results for the CME conductivity in the quenched theory, both with Wilson and staggered fermions. The conductivity is consistent with zero in all the cases (within 2σ) even without taking the continuum limit.

artifact of using a non-conserved vector current.

Finally, we note that in the quenched ensembles gluon configurations in different Polyakov loop sectors contribute. Contrary to the case of the CSE in the quenched approximation [33], the Polyakov loop backgrounds do not affect the CME conductivity appreciably. This is because the complex Polyakov loop backgrounds effectively amount to an imaginary baryon chemical potential, and therefore only affect the baryon density (entering the CSE) but not the chiral density.

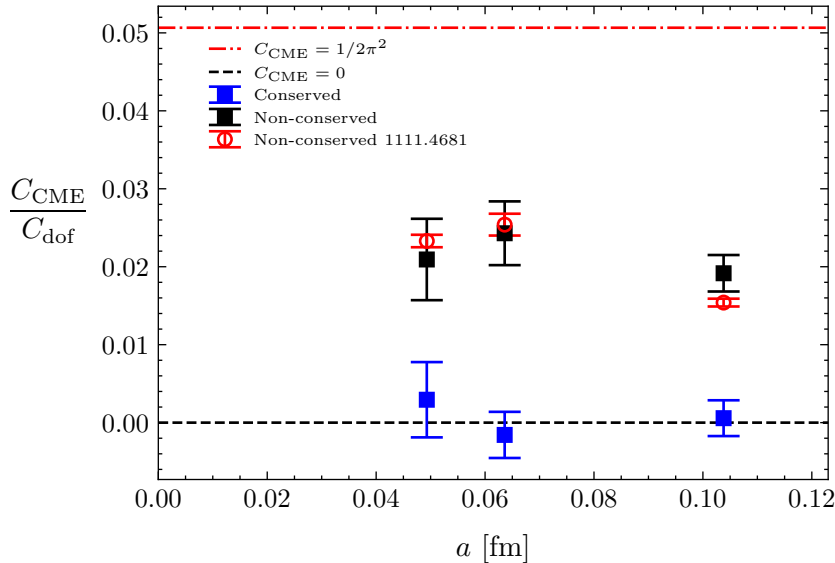


Figure 6: Direct comparison of the study in [21] (open red circles), with our setup with a conserved vector current (filled blue squares) and a non-conserved one (filled black squares). The results with non-conserved currents agree with each other within errors and deviate from the correct value. The result with a conserved vector current is consistent with a vanishing C_{CME} .

4.3 QCD at physical quark masses

Finally, we present our results for C_{CME} in full QCD using $2 + 1$ flavors of staggered fermions with physical quark masses. The measurements were performed on an already existing ensemble of configurations for different magnetic fields [49, 59].

In Fig. 7, we present the dependence of the conductivity on the temperature using several finite-temperature lattice ensembles $24^3 \times 6$, $24^3 \times 8$, $28^3 \times 10$, $36^3 \times 12$ as well as two zero-temperature ensembles $24^3 \times 32$ and $32^3 \times 48$. The CME coefficient vanishes for all temperatures within errors. We also present the continuum limit for temperatures from 100 MeV to 400 MeV, considering a spline fit procedure combined with the continuum extrapolation. In particular, we consider a T -dependent spline fit of all lattice points with a -dependent coefficients of order a^2 . By minimizing the χ^2/dof , the optimal fitting surface in the $a - T$ plane is found (see [60] for further details). The statistical error of this procedure is calculated using the jackknife samples, while we estimate the systematic error by repeating several times the spline fit removing the coarsest lattice and including $\mathcal{O}(a^4)$ coefficients. The maximum difference between the continuum limits obtained with these data sets and the original one is taken as the systematic error, which is added in quadrature to the statistical one. The so-obtained continuum extrapolation is again compatible with zero at all temperatures.

We mention that both the chiral chemical potential and the vector current may be defined with different flavor quantum numbers, i.e. baryon number, electric charge or “light baryon number”, cf. Ref. [33]. We checked that C_{CME} vanishes for any combination of

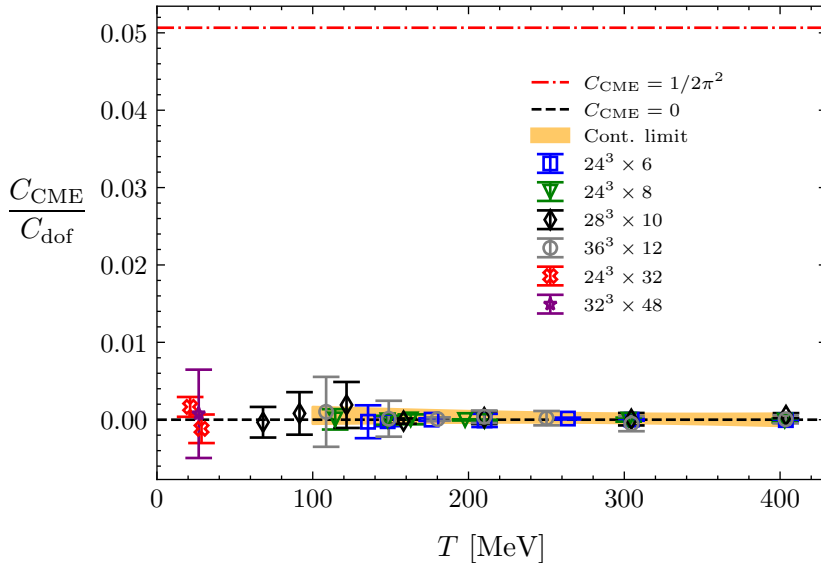


Figure 7: Full dynamic QCD results with 2+1 flavors of staggered fermions at the physical point in a wide range of temperatures. The continuum limit for points at $T > 100$ MeV is shown as an orange band.

these as well. This is expected, since the general argument implying that CME vanishes in equilibrium, applies in all the different setups.

These vanishing results constitute an important check, since they show that the arguments presented at the beginning of this work and in the literature also apply to QCD. In addition, they show that the implications of Bloch’s theorem, derived for ground states at zero temperature, also generalize to our nonzero temperature setting.

In Fig. 8, we show the results for the chiral susceptibility χ_5 in full QCD for different temperatures. Since the renormalization² of the observable requires a zero temperature subtraction, approaching the continuum limit is computationally more challenging than for C_{CME} . For this reason, we only present results for $N_t = 6, 8$ lattices with different volumes. To reduce cutoff effects, we follow a similar improvement program for the observable as in Ref. [46]. We multiply our results by the improvement coefficients, which can be calculated for very high temperatures (free quarks with $m/T \approx 0$) for the different values of N_t . In particular, we find these coefficients to be 1.2505 for $N_t = 6$ and 1.1196 for $N_t = 8$. The susceptibility starts growing around the crossover temperature T_c , and it slowly approaches the analytic result for massless free fermions. The asymptotic limit seems to be reached at temperatures higher than 1 GeV, a similar behavior as observed in the QCD pressure [46], and in contrast with the fast increase after T_c observed in the CSE conductivity [61].

²We note here that χ_5 is also subject to multiplicative renormalization, in particular by the same factor (squared) as the flavor-singlet axial vector current in the CSE [33]. This renormalization constant approaches unity both for Wilson and for staggered fermions in the continuum limit [47, 48] and it could be used to further improve the scaling of the observable.

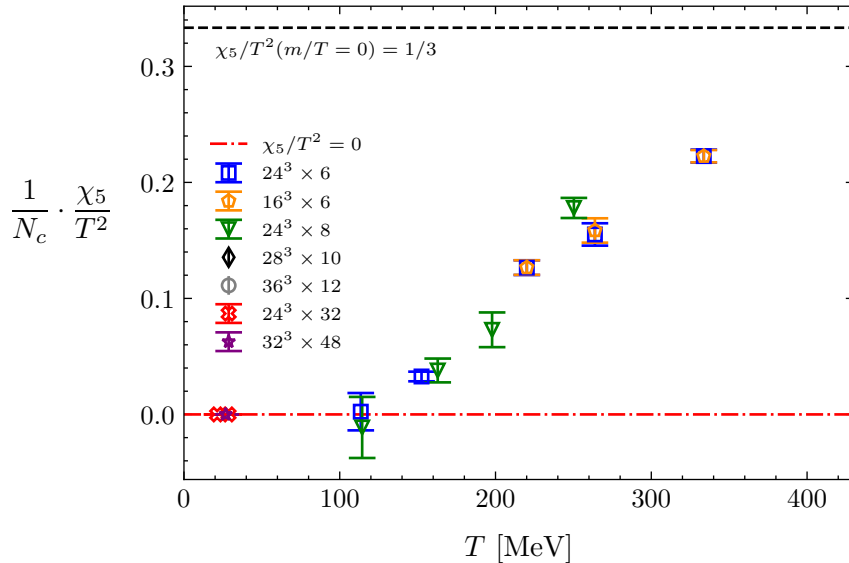


Figure 8: Axial susceptibility for 2 + 1 flavors of staggered quarks in full QCD at the physical point. The results are normalized by the number of colors $N_c = 3$ in order to directly compare to the free fermions result (2.18). We observe χ_5 to slowly grow above the crossover temperature, approaching the analytic result for massless non-interacting fermions (indicated by the black dashed line).

5 Summary and outlook

In this paper, we have presented a complete characterization of the absence of the chiral magnetic effect in thermal equilibrium. We carefully showed how regularization plays a crucial role in the calculation, in particular, for the first-order Taylor coefficient of the conductivity C_{CME} . We also reviewed how chiral imbalance is indeed induced by a chiral chemical potential μ_5 , even when this parameter does not couple to a conserved quantity in the theory.

By using first-principles Euclidean lattice calculations, we showed how using the appropriate discretization of the conserved currents leads to a vanishing CME conductivity for non-interacting fermions, using both Wilson and staggered quarks. At the same time chirality is indeed present in the system with both discretizations, indicated by a non-vanishing χ_5 . We then moved to the quenched theory, where we again observed the absence of the CME. We also directly compared to the earlier results of Ref. [21], where a non-vanishing CME conductivity has been found, albeit with a non-conserved vector current. The comparison shows that the use of a conserved vector current is vital to obtain consistent results. Finally, we presented the first results in full dynamical QCD at the physical point, using 2 + 1 flavors of staggered fermions, for a wide range of temperatures. These results, which have been continuum extrapolated, are completely consistent with $C_{\text{CME}} = 0$. In addition, we calculated χ_5 in the same setup, exhibiting an increase above the QCD crossover temperature, slowly approaching the non-interacting quarks limit.

Once the equilibrium effect is completely understood, it is natural to extend this study to the out-of-equilibrium conductivity. To access the latter, we would need information about the spectral function, which is accessible via lattice simulations using spectral reconstruction methods. This technique has already been employed to indirectly study the CME in Ref. [30] as a contribution to the electric conductivity. Using the temporal correlator between vector and axial vector currents one would have access to the out-of-equilibrium C_{CME} in QCD, which potentially provides information on how the out-of-equilibrium CME is affected by interactions. A first step in this direction has been taken in Ref. [24], where the role of the regularization and the relation between Euclidean and retarded correlators has been discussed.

Acknowledgments

This research was funded by the DFG (Collaborative Research Center CRC-TR 211 “Strong-interaction matter under extreme conditions” - project number 315477589 - TRR 211) and by the Helmholtz Graduate School for Hadron and Ion Research (HGS-HIRE for FAIR). The authors are grateful for inspiring discussions with Pavel Buividovich, Kenji Fukushima, Keh-Fei Liu, Ho-Ung Yee, Dirk Rischke, Sören Schlichting, Ilya Selyuzhenkov, Igor Shovkovy and Lorenz von Smekal.

A Parameterization dependence of the unregularized C_{CME} in the free case

In this appendix we will analyze the integral appearing in (2.15) in order to show that without an a priori regularization process the CME coefficient is mathematically ill-defined despite not containing UV divergences. We start by defining two contributions

$$f_m = \frac{1}{4\pi^3} \int_{-\infty}^{\infty} dp_3 dp_4 \frac{m_s^2}{(m_s^2 + p_4^2 + p_3^2)^2} \quad (\text{A.1})$$

and

$$f_p = \frac{1}{4\pi^3} \int_{-\infty}^{\infty} dp_3 dp_4 \frac{p_4^2 - p_3^2}{(m_s^2 + p_4^2 + p_3^2)^2}, \quad (\text{A.2})$$

with which (2.15) is just

$$C_{\text{CME}} = \sum_{s=0}^3 c_s (f_m + f_p). \quad (\text{A.3})$$

The first term, f_m , is a well behaved integral with the value

$$f_m = \frac{1}{4\pi^2}. \quad (\text{A.4})$$

In turn, f_p depends on the way one parameterizes the integral over the $p_3 - p_4$ plane. First of all, notice that performing the p_3 and p_4 integrals in a different order gives different

results,

$$f_{p,34} = \frac{1}{4\pi^3} \int_{-\infty}^{\infty} dp_3 \left(\int_{-\infty}^{\infty} dp_4 \frac{p_4^2 - p_3^2}{(m_s^2 + p_4^2 + p_3^2)^2} \right) = \frac{1}{4\pi^3} \int_{-\infty}^{\infty} dp_3 \frac{\pi}{2(m_s^2 + p_3^2)^{3/2}} = \frac{1}{4\pi^2}, \quad (\text{A.5})$$

while

$$f_{p,43} = \frac{1}{4\pi^3} \int_{-\infty}^{\infty} dp_4 \left(\int_{-\infty}^{\infty} dp_3 \frac{p_4^2 - p_3^2}{(m_s^2 + p_4^2 + p_3^2)^2} \right) = \frac{1}{4\pi^3} \int_{-\infty}^{\infty} dp_4 \frac{-\pi}{2(m_s^2 + p_4^2)^{3/2}} = -\frac{1}{4\pi^2}. \quad (\text{A.6})$$

More generally, one can rotate the integration variables

$$\begin{pmatrix} p_3 \\ p_4 \end{pmatrix} = \begin{pmatrix} \cos \alpha & \sin \alpha \\ -\sin \alpha & \cos \alpha \end{pmatrix} \begin{pmatrix} u \\ v \end{pmatrix} \quad (\text{A.7})$$

to find that depending on the (arbitrary) rotation angle α , the result changes continuously between the two extremes (A.5) and (A.6),

$$f_{p,\alpha} = -\frac{\cos 2\alpha}{4\pi^2}. \quad (\text{A.8})$$

Taking for example $\alpha = \pi/2$, i.e. considering the ordering $f_{p,34}$, results in the value $1/(2\pi^2)$ for the unregularized contribution of the $s = 0$ field to C_{CME} .

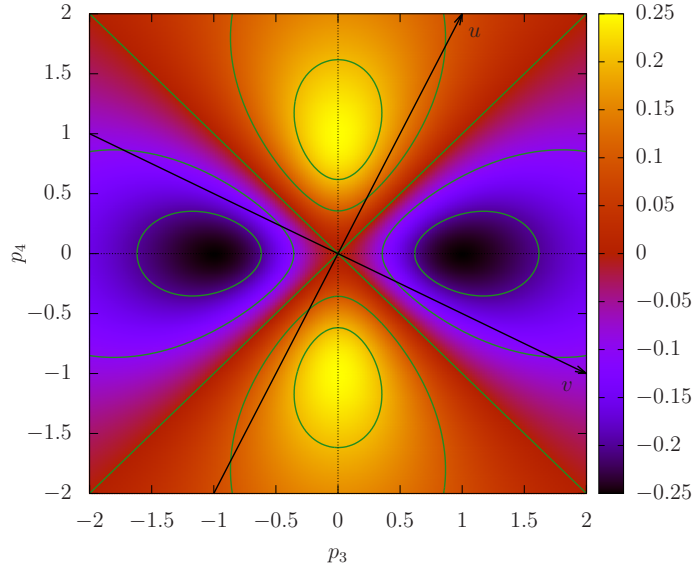


Figure 9: The heat map of the integrand of f_p as defined in (A.2). A few contours are highlighted in green for better visibility, while an example of the variable change in (A.8) is shown by the rotated coordinate system (black).

The heat map of the integrand of f_p for $m_s = 1$ is shown in Fig. 9, with an example change of coordinates, illustrating how the different results arise. To understand the origin

of this ambiguity, it is instructive to use polar coordinates (p, φ) , writing

$$f_p = \frac{1}{4\pi^3} \int_0^\infty dp \int_0^{2\pi} d\varphi \frac{p^3 \cos 2\varphi}{(m_s^2 + p^2)^2}, \quad (\text{A.9})$$

which highlights the fact that there are divergent directions (in fact almost all of them are), since the integrand only falls off as p^{-1} for large p . However, integrating over φ combines them in such a way that cancellations occur to make it possibly finite. This completes our illustration of the ill-definedness of f_p and hence the unregularized value of C_{CME} .

As a final remark, evaluating the sum over the PV fields always leads to a well defined integral, which is easiest to see for the form of f_p in polar coordinates, where the integrand falls off faster for $p \gg m_s$ owing to the PV subtraction,

$$\sum_{s=0}^3 c_s f_p = \frac{1}{4\pi^3} \int_0^\infty dp \int_0^{2\pi} d\varphi \sum_{s=0}^3 c_s \frac{p^3 \cos 2\varphi}{(m_s^2 + p^2)^2} \quad (\text{A.10})$$

$$= \frac{1}{4\pi^3} \int_0^\infty dp \int_0^{2\pi} d\varphi \left(3 \frac{m^4 + m_1^4 - 2m_2^4}{p^5} + \mathcal{O}(p^{-7}) \right) \cos 2\varphi, \quad (\text{A.11})$$

and vanishes due to the φ -integral. Here we inserted the specific PV masses (2.8).

B CME in the free case from the two-point function at finite temperature

In this appendix, we generalize the calculation of Sec. 2.2 to finite temperatures T . This is done in a straightforward manner, by replacing the frequency component of the integral by a sum over fermionic Matsubara frequencies,

$$\int \frac{dp_0}{2\pi} \rightarrow iT \sum_{n=-\infty}^{\infty}, \quad (\text{B.1})$$

while also replacing $p_0 \rightarrow i\omega_n = i2\pi T(n + 1/2)$ in $\tilde{S}_s(p)$. Doing so in Eq. (2.14), yields

$$C_{\text{CME}qB} = -\frac{qB}{2\pi^2} \sum_{s=0}^3 c_s T \sum_{n=-\infty}^{\infty} \int_{-\infty}^{\infty} dp_3 \int_0^\infty dZ_1 dZ_2 e^{-(Z_1+Z_2)(\omega_n^2+m_s^2+p_3^2)} (m_s^2 + \omega_n^2 - p_3^2). \quad (\text{B.2})$$

The linear magnetic field dependence is again obtained, which allows the simplification of the expression. Doing the p_3 integral results in

$$C_{\text{CME}} = -\frac{T}{2\pi^{3/2}} \sum_{s=0}^3 c_s \int_0^\infty dZ_1 dZ_2 \sum_{n=-\infty}^{\infty} e^{-(Z_1+Z_2)(\omega_n^2+m_s^2)} \left[\frac{m_s^2 + \omega_n^2}{\sqrt{Z_1 + Z_2}} - \frac{1}{2(Z_1 + Z_2)^{3/2}} \right]. \quad (\text{B.3})$$

The Z_1, Z_2 integrals can be performed for all terms of the sum, e.g. by changing variables to $Z_1 = \frac{\alpha+\beta}{2}$ and $Z_2 = \frac{\alpha-\beta}{2}$. The final result is again zero, now for all temperatures.

C Axial susceptibility in the free case

In this appendix we calculate the axial susceptibility (2.16) in the free case. First, we discuss χ_5 at $T = 0$ in order to illustrate that this observable is subject to additive renormalization. We consider the second derivative of the partition function with respect to μ_5 again in the PV regularization,

$$\chi_5^b = i \sum_{s=0}^3 c_s \int \frac{d^4 k}{(2\pi)^4} \frac{\text{Tr}[\gamma_0 \gamma_5 (\not{k} + m_s) \gamma_0 \gamma_5 (\not{k} + m_s)]}{(k^2 - m_s^2)^2}. \quad (\text{C.1})$$

Carrying out the traces and using the Schwinger parameterization

$$\chi_5^b = 4i \sum_{s=0}^3 c_s \int_0^\infty dt \int \frac{d^4 k}{(2\pi)^4} (2k_0^2 - k^2 - m^2) t e^{-t(m_s^2 - k^2)}. \quad (\text{C.2})$$

The momentum integrals can be solved, yielding

$$\chi_5^b = \frac{1}{4\pi^2} \sum_{s=0}^3 c_s \int_0^\infty dt \left[-\frac{1}{t^2} + \frac{m_s^2}{t} \right] e^{-t(m_s^2 - k^2)}. \quad (\text{C.3})$$

This integral is divergent for the physical species $s = 0$, but it is regularized by the PV copies. The final result after integration reads

$$\chi_5^b = -\frac{1}{2\pi^2} \sum_{s=0}^3 c_s m_s^2 \log\left(\frac{m_s^2}{m^2}\right) = -\frac{1}{2\pi^2} \left[\log(4)\Lambda^2 - m^2 \left[1 + \log\left(\frac{\Lambda^2}{2m^2}\right) \right] + \mathcal{O}(\Lambda^{-2}) \right], \quad (\text{C.4})$$

where we inserted the specific form (2.8) of the PV masses, noting that the physical mass is $m = m_0$. Here we explicitly see how the introduction of μ_5 leads to a quadratic divergence (plus a logarithmic one) in $\log \mathcal{Z}$. This motivates the $T = 0$ subtraction of the bare observable in (2.17).

To calculate the finite temperature result, is again enough to use the Matsubara formalism. From Eq. (C.1) and rotating to imaginary time, we get

$$\chi_5^T = -4T \sum_{n=-\infty}^{\infty} \int \frac{d^3 k}{(2\pi)^3} \frac{(i\omega_n)^2 + \vec{k}^2 - m^2}{[(i\omega_n)^2 - \vec{k}^2 - m^2]^2}. \quad (\text{C.5})$$

It is straightforward to evaluate the Matsubara sum, yielding, for the T -dependent part,

$$\chi_5 = \frac{4}{\pi^2} \int dk \frac{k^2}{E_k} n_F(E_k), \quad (\text{C.6})$$

which is Eq. (2.18).

D CME with free staggered fermions

In this appendix, we illustrate how to calculate C_{CME} for free staggered quarks using explicitly the eigenvalues and eigenvectors of the Dirac operator. The discussion closely follows the analogous method that we developed for the CSE [33]. To describe free quarks, we turn off the gluon fields and consider one color component only. We discuss a single quark flavor with mass m , the chemical potential μ_5 and the vector current J_3 . Below we work on an $N_s^3 \times N_t$ lattice and write everything in lattice units, setting $a = 1$. In the non-interacting theory, the disconnected term of Eq. (3.11) vanishes, so we only need to calculate two terms

$$\left. \frac{\partial J_3}{\partial \mu_5} \right|_{\mu_5=0} = \frac{1}{N_s^3 N_t} \left[-\frac{1}{4} \text{Tr}(\Gamma_3 M^{-1} \Gamma_{45} M^{-1}) + \frac{1}{4} \text{Tr} \left(\frac{\partial \Gamma_3}{\partial \mu_5} M^{-1} \right) \right], \quad (\text{D.1})$$

and the expectation value indicating the fermion path integral was omitted for brevity.

The massless staggered Dirac operator has purely imaginary eigenvalues, due to its antihermiticity. Moreover, due to staggered chiral symmetry, $\{\not{D}, \eta_5\} = 0$ (with $\eta_5 = (-1)^{n_1+n_2+n_3+n_4}$), the eigenvalues come in complex conjugate pairs,

$$\not{D}\Psi_i = \pm i\lambda_i\Psi_i. \quad (\text{D.2})$$

When the mass is included, we will need the analogous eigensystem for $MM^\dagger = (\not{D} + m)(\not{D} + m)^\dagger = \not{D}\not{D}^\dagger + m^2$, so

$$MM^\dagger\Psi_i = (\lambda_i^2 + m^2)\Psi_i, \quad (\text{D.3})$$

where each eigenvalue is doubly degenerate due to (D.2). Using this eigensystem as basis, the traces in Eq. (D.1) can be written as

$$\begin{aligned} \left. \frac{\partial J_3}{\partial \mu_5} \right|_{\mu_5=0} = \frac{1}{N_s^3 N_t} & \left[-\frac{1}{4} \sum_{i,j} \frac{1}{(\lambda_i^2 + m^2)(\lambda_j^2 + m^2)} \Psi_i^\dagger \Gamma_3 M^\dagger \Psi_j \Psi_j^\dagger \Gamma_{45} M^\dagger \Psi_i \right. \\ & \left. + \frac{1}{4} \sum_i \frac{1}{\lambda_i^2 + m^2} \Psi_i^\dagger \frac{\partial \Gamma_3}{\partial \mu_5} M^\dagger \Psi_i \right], \end{aligned} \quad (\text{D.4})$$

where we inserted a complete set of eigenstates $\sum_j \Psi_j \Psi_j^\dagger = \mathbb{1}$ in the first term and used $M^{-1} = M^\dagger (MM^\dagger)^{-1}$.

Next, the separability of the problem allows us to reduce Eq. (D.3) to one two-dimensional and two one-dimensional eigenproblems. This will enable us to determine the complete spectrum on much larger lattices than with a direct, four-dimensional approach. To this end, we write the free Dirac operator (at $\mu_5 = 0$) as $\not{D} = \not{D}_{12} + \not{D}_3 + \not{D}_4$ with $\not{D}_{12} = \not{D}_1 + \not{D}_2$ and

$$\not{D}_\nu(n, m) = \frac{\eta_\nu(n)}{2} [u_\nu(n)\delta_{n+\hat{\nu},m} - u_\nu^*(n-\hat{\nu})\delta_{n-\hat{\nu},m}] \equiv \eta_\nu(n)D_\nu(n, m). \quad (\text{D.5})$$

Similarly, the staggered Dirac matrices (3.4) (at $\mu_5 = 0$) simplify to

$$\Gamma_\nu(n, m) = \frac{\eta_\nu(n)}{2} [u_\nu(n)\delta_{n+\hat{\nu},m} + u_\nu^*(n-\hat{\nu})\delta_{n-\hat{\nu},m}] \equiv \eta_\nu(n)S_\nu(n, m). \quad (\text{D.6})$$

Notice that the hop operators satisfy

$$[S_1, S_3] = [S_1, S_4] = [S_2, S_3] = [S_2, S_4] = [S_3, S_4] = 0, \quad (\text{D.7})$$

because the $U(1)$ links only enter in S_1 and S_2 .

The squared operator $MM^\dagger = MM_{12}^\dagger + MM_3^\dagger + MM_4^\dagger$ separates into three terms that act in the respective subspaces and only depend on the respective coordinates – thus they commute with each other. Therefore, the eigenvectors in (D.3) factorize,

$$\Psi_{\{i_{12}, i_3, i_4\}}(n_1, n_2, n_3, n_4) = \rho_{i_{12}}(n_1, n_2) \phi_{i_3}(n_3) \xi_{i_4}(n_4), \quad (\text{D.8})$$

with $0 \leq i_{12} < N_s^2$, $0 \leq i_3 < N_s$ and $0 \leq i_4 < N_t$.³ Below we use a shorthand notation and simply write $\Psi_i = \rho_i \phi_i \xi_i$.

We proceed by expanding the operators appearing in the matrix elements in Eq. (D.4) into separate contributions that depend only on $n_{1,2}$, n_3 or n_4 ,

$$\Gamma_3 = (-1)^{n_1+n_2} S_3, \quad (\text{D.9})$$

$$M^\dagger = -\not{D}_{12} - (-1)^{n_1+n_2} D_3 - (-1)^{n_1+n_2+n_3} D_4 + m, \quad (\text{D.10})$$

and it can be shown with some algebra and Eq. (D.7) that

$$\Gamma_{45} = -S_{12} S_3 (-1)^{n_2}, \quad (\text{D.11})$$

with $S_{12} = \{S_1, S_2\}/2$. Finally, for the tadpole term we need the derivative of Γ_3 with respect to the chiral chemical potential. Using (3.4) and (3.7),

$$\frac{\partial \Gamma_3}{\partial \mu_5} = -S_{12} D_3 (-1)^{n_2}. \quad (\text{D.12})$$

The necessary products, appearing in (D.4) are therefore

$$\begin{aligned} \Gamma_3 M^\dagger &= -[(-1)^{n_1+n_2} \not{D}_{12}]_{12} \cdot [S_3]_3 \cdot [\mathbf{1}]_4 \\ &\quad - [\mathbf{1}]_{12} \cdot [S_3 D_3]_3 \cdot [\mathbf{1}]_4 \\ &\quad - [\mathbf{1}]_{12} \cdot [S_3 (-1)^{n_3}]_3 \cdot [D_4]_4 \\ &\quad + m [(-1)^{n_1+n_2}]_{12} \cdot [S_3]_3 \cdot [\mathbf{1}]_4, \end{aligned} \quad (\text{D.13})$$

where $[\cdot]_{12}$, $[\cdot]_3$ and $[\cdot]_4$ indicate operators that only act in the respective spaces and only depend on the respective coordinates. Similarly, we obtain

$$\begin{aligned} \Gamma_{45} M^\dagger &= +[S_{12} (-1)^{n_2} \not{D}_{12}]_{12} \cdot [S_3]_3 \cdot [\mathbf{1}]_4 \\ &\quad + [S_{12} (-1)^{n_1}]_{12} \cdot [S_3 D_3]_3 \cdot [\mathbf{1}]_4 \\ &\quad + [S_{12} (-1)^{n_1}]_{12} \cdot [S_3 (-1)^{n_3}]_3 \cdot [D_4]_4 \\ &\quad - m [S_{12} (-1)^{n_2}]_{12} \cdot [S_3]_3 \cdot [\mathbf{1}]_4, \end{aligned} \quad (\text{D.14})$$

³Note that the same separation does not hold for the eigensystem (D.2), since for example $[\not{D}_{12}, \not{D}_3] \neq 0$ due to the staggered phases. This is because $[MM^\dagger, \eta_5] = 0$ but $[\not{D}, \eta_5] \neq 0$.

and

$$\begin{aligned}
\frac{\partial \Gamma_3}{\partial \mu_5} M^\dagger = & + [S_{12}(-1)^{n_2} \not{D}_{12}]_{12} \cdot [D_3]_3 \cdot [\mathbf{1}]_4 \\
& + [S_{12}(-1)^{n_1}]_{12} \cdot [D_3 D_3]_3 \cdot [\mathbf{1}]_4 \\
& + [S_{12}(-1)^{n_1}]_{12} \cdot [D_3(-1)^{n_3}]_3 \cdot [D_4]_4 \\
& - m[S_{12}(-1)^{n_2}]_{12} \cdot [D_3]_3 \cdot [\mathbf{1}]_4 .
\end{aligned} \tag{D.15}$$

Combining everything, Eq. (D.4) becomes

$$\begin{aligned}
\left. \frac{\partial J_3}{\partial \mu_5} \right|_{\mu_5=0} = & + \frac{1}{N_s^3 N_t} \frac{1}{4} \sum_{i,j} \frac{1}{(\lambda_i^2 + m^2)(\lambda_j^2 + m^2)} \\
& \left\{ [A_{ij} C_{ji}]_{12} \cdot [G_{ij} G_{ji}]_3 \cdot [\delta_{ij}]_4 + [A_{ij} E_{ji}]_{12} \cdot [G_{ij} H_{ji}]_3 \cdot [\delta_{ij}]_4 \right. \\
& + [A_{ij} E_{ji}]_{12} \cdot [G_{ij} I_{ji}]_3 \cdot [\delta_{ij} J_{ji}]_4 - m[A_{ij} F_{ji}]_{12} \cdot [G_{ij} G_{ji}]_4 \cdot [\delta_{ij}]_4 \\
& + [\delta_{ij} C_{ji}]_{12} \cdot [H_{ij} G_{ji}]_3 \cdot [\delta_{ij}]_4 + [\delta_{ij} E_{ji}]_{12} \cdot [H_{ij} H_{ji}]_4 \cdot [\delta_{ij}]_4 \\
& + [\delta_{ij} E_{ji}]_{12} \cdot [H_{ij} I_{ji}]_3 \cdot [\delta_{ij} J_{ji}]_4 - m[\delta_{ij} F_{ji}]_{12} \cdot [H_{ij} G_{ji}]_4 \cdot [\delta_{ij}]_4 \\
& + [\delta_{ij} C_{ji}]_{12} \cdot [I_{ij} G_{ji}]_3 \cdot [J_{ij} \delta_{ji}]_4 + [\delta_{ij} E_{ji}]_{12} \cdot [I_{ij} H_{ji}]_3 \cdot [J_{ij} \delta_{ij}]_4 \\
& + [\delta_{ij} E_{ji}]_{12} \cdot [I_{ij} I_{ji}]_3 \cdot [J_{ij} J_{ji}]_4 - m[\delta_{ij} F_{ji}]_{12} \cdot [I_{ij} G_{ji}]_3 \cdot [J_{ij} \delta_{ij}]_4 \\
& - m[B_{ij} C_{ji}]_{12} \cdot [G_{ij} G_{ji}]_3 \cdot [\delta_{ij}]_4 - m[B_{ij} E_{ji}]_{12} \cdot [G_{ij} H_{ji}]_3 \cdot [\delta_{ij}]_4 \\
& \left. - m[B_{ij} E_{ji}]_{12} \cdot [G_{ij} I_{ji}]_3 \cdot [\delta_{ij} J_{ji}]_4 + m^2[B_{ij} F_{ji}]_{12} \cdot [G_{ij} G_{ji}]_3 \cdot [\delta_{ij}]_4 \right\} \\
& + \frac{1}{N_s^3 N_t} \frac{1}{4} \sum_i \frac{1}{\lambda_i^2 + m^2} \\
& \left\{ [C_{ii}]_{12} \cdot [K_{ii}]_3 \cdot [\delta_{ii}]_4 + [E_{ii}]_{12} \cdot [N_{ii}]_3 \cdot [J_{ii}]_4 \right. \\
& \left. + [E_{ii}]_{12} \cdot [L_{ii}]_3 \cdot [\delta_{ii}]_4 - m[F_{ii}]_{12} \cdot [K_{ii}]_3 \cdot [\delta_{ii}]_4 \right\} ,
\end{aligned} \tag{D.16}$$

with

$$\begin{aligned}
A_{ij} & \equiv \rho_i^\dagger (-1)^{n_1+n_2} \not{D}_{12} \rho_j , & B_{ij} & \equiv \rho_i^\dagger (-1)^{n_1+n_2} \rho_j , \\
C_{ij} & \equiv \rho_i^\dagger S_{12} (-1)^{n_2} \not{D}_{12} \rho_j , & E_{ij} & \equiv \rho_i^\dagger S_{12} (-1)^{n_1} \rho_j , \\
F_{ij} & \equiv \rho_i^\dagger S_{12} (-1)^{n_2} \rho_j , & J_{ij} & \equiv \xi_i^\dagger D_4 \xi_j , \\
G_{ij} & \equiv \phi_i^\dagger S_3 \phi_j , & H_{ij} & \equiv \phi_i^\dagger S_3 D_3 \phi_j , \\
I_{ij} & \equiv \phi_i^\dagger S_3 (-1)^{n_3} \phi_j , & K_{ij} & \equiv \phi_i^\dagger D_3 \phi_j , \\
L_{ij} & \equiv \phi_i^\dagger D_3 D_3 \phi_j , & N_{ij} & \equiv \phi_i^\dagger D_3 (-1)^{n_3} \phi_j .
\end{aligned} \tag{D.17}$$

To solve the eigenvalue problems, a two-dimensional one in the 12 plane in the presence of the magnetic field and two one-dimensional ones in the 3 and 4 directions, we use the LAPACK library. The eigensystem of the former problem gives Hofstadter's butterfly [62], the spectrum of a well-known solid-state physics model. Its importance for lattice QCD has been pointed out in Ref. [63], and it has been generalized both for gluonic interactions [64,

[65] as well as for inhomogeneous magnetic fields [61]. The value for the current derivative can be reconstructed using Eq. (D.16), and C_{CME} can be extracted in the same way as explained in the main text by calculating the observable at different values of the magnetic field.

References

- [1] D.E. Kharzeev, *The Chiral Magnetic Effect and Anomaly-Induced Transport*, *Prog. Part. Nucl. Phys.* **75** (2014) 133 [[1312.3348](#)].
- [2] X.-G. Huang, *Electromagnetic fields and anomalous transports in heavy-ion collisions — A pedagogical review*, *Rept. Prog. Phys.* **79** (2016) 076302 [[1509.04073](#)].
- [3] K. Landsteiner, *Notes on Anomaly Induced Transport*, *Acta Phys. Polon. B* **47** (2016) 2617 [[1610.04413](#)].
- [4] D.E. Kharzeev, L.D. McLerran and H.J. Warringa, *The Effects of topological charge change in heavy ion collisions: 'Event by event P and CP violation'*, *Nucl. Phys. A* **803** (2008) 227 [[0711.0950](#)].
- [5] K. Fukushima, D.E. Kharzeev and H.J. Warringa, *The Chiral Magnetic Effect*, *Phys. Rev. D* **78** (2008) 074033 [[0808.3382](#)].
- [6] Q. Li, D.E. Kharzeev, C. Zhang, Y. Huang, I. Pletikosic, A.V. Fedorov et al., *Observation of the chiral magnetic effect in ZrTe5*, *Nature Phys.* **12** (2016) 550 [[1412.6543](#)].
- [7] STAR collaboration, *Fluctuations of charge separation perpendicular to the event plane and local parity violation in $\sqrt{s_{NN}} = 200$ GeV Au+Au collisions at the BNL Relativistic Heavy Ion Collider*, *Phys. Rev. C* **88** (2013) 064911 [[1302.3802](#)].
- [8] STAR collaboration, *Beam-energy dependence of charge separation along the magnetic field in Au+Au collisions at RHIC*, *Phys. Rev. Lett.* **113** (2014) 052302 [[1404.1433](#)].
- [9] STAR collaboration, *Search for the chiral magnetic effect with isobar collisions at $\sqrt{s_{NN}}=200$ GeV by the STAR Collaboration at the BNL Relativistic Heavy Ion Collider*, *Phys. Rev. C* **105** (2022) 014901 [[2109.00131](#)].
- [10] K. Kamada, N. Yamamoto and D.-L. Yang, *Chiral effects in astrophysics and cosmology*, *Prog. Part. Nucl. Phys.* **129** (2023) 104016 [[2207.09184](#)].
- [11] N. Yamamoto, *Chiral transport of neutrinos in supernovae: Neutrino-induced fluid helicity and helical plasma instability*, *Phys. Rev. D* **93** (2016) 065017 [[1511.00933](#)].
- [12] K. Fukushima, M. Ruggieri and R. Gatto, *Chiral magnetic effect in the PNJL model*, *Phys. Rev. D* **81** (2010) 114031 [[1003.0047](#)].
- [13] V.A. Miransky and I.A. Shovkovy, *Quantum field theory in a magnetic field: From quantum chromodynamics to graphene and Dirac semimetals*, *Phys. Rept.* **576** (2015) 1 [[1503.00732](#)].
- [14] H.-U. Yee, *Holographic Chiral Magnetic Conductivity*, *JHEP* **11** (2009) 085 [[0908.4189](#)].
- [15] A. Rebhan, A. Schmitt and S.A. Stricker, *Anomalies and the chiral magnetic effect in the Sakai-Sugimoto model*, *JHEP* **01** (2010) 026 [[0909.4782](#)].
- [16] A. Gynther, K. Landsteiner, F. Pena-Benitez and A. Rebhan, *Holographic Anomalous Conductivities and the Chiral Magnetic Effect*, *JHEP* **02** (2011) 110 [[1005.2587](#)].

- [17] A.V. Sadofyev and M.V. Isachenkov, *The Chiral magnetic effect in hydrodynamical approach*, *Phys. Lett. B* **697** (2011) 404 [[1010.1550](#)].
- [18] S. Shi, Y. Jiang, E. Lilleskov and J. Liao, *Anomalous Chiral Transport in Heavy Ion Collisions from Anomalous-Viscous Fluid Dynamics*, *Annals Phys.* **394** (2018) 50 [[1711.02496](#)].
- [19] K. Hattori, Y. Hidaka and D.-L. Yang, *Axial Kinetic Theory and Spin Transport for Fermions with Arbitrary Mass*, *Phys. Rev. D* **100** (2019) 096011 [[1903.01653](#)].
- [20] A. Yamamoto, *Chiral magnetic effect in lattice QCD with a chiral chemical potential*, *Phys. Rev. Lett.* **107** (2011) 031601 [[1105.0385](#)].
- [21] A. Yamamoto, *Lattice study of the chiral magnetic effect in a chirally imbalanced matter*, *Phys. Rev. D* **84** (2011) 114504 [[1111.4681](#)].
- [22] P.V. Buividovich, *Anomalous transport with overlap fermions*, *Nucl. Phys. A* **925** (2014) 218 [[1312.1843](#)].
- [23] N. Müller, S. Schlichting and S. Sharma, *Chiral magnetic effect and anomalous transport from real-time lattice simulations*, *Phys. Rev. Lett.* **117** (2016) 142301 [[1606.00342](#)].
- [24] P.V. Buividovich, *Out-of-equilibrium Chiral Magnetic Effect from simulations on Euclidean lattices*, [2404.14263](#).
- [25] P.V. Buividovich, M.N. Chernodub, E.V. Luschevskaya and M.I. Polikarpov, *Numerical evidence of chiral magnetic effect in lattice gauge theory*, *Phys. Rev. D* **80** (2009) 054503 [[0907.0494](#)].
- [26] M. Abramczyk, T. Blum, G. Petropoulos and R. Zhou, *Chiral magnetic effect in 2+1 flavor QCD+QED*, *PoS LAT2009* (2009) 181 [[0911.1348](#)].
- [27] P.V. Buividovich, M.N. Chernodub, E.V. Luschevskaya and M.I. Polikarpov, *Quark electric dipole moment induced by magnetic field*, *Phys. Rev. D* **81** (2010) 036007 [[0909.2350](#)].
- [28] V.V. Braguta, P.V. Buividovich, T. Kalaydzhyan, S.V. Kuznetsov and M.I. Polikarpov, *The Chiral Magnetic Effect and chiral symmetry breaking in SU(3) quenched lattice gauge theory*, *Phys. Atom. Nucl.* **75** (2012) 488 [[1011.3795](#)].
- [29] G.S. Bali, F. Bruckmann, G. Endrődi, Z. Fodor, S.D. Katz and A. Schäfer, *Local CP-violation and electric charge separation by magnetic fields from lattice QCD*, *JHEP* **04** (2014) 129 [[1401.4141](#)].
- [30] N. Astrakhantsev, V.V. Braguta, M. D'Elia, A.Y. Kotov, A.A. Nikolaev and F. Sanfilippo, *Lattice study of the electromagnetic conductivity of the quark-gluon plasma in an external magnetic field*, *Phys. Rev. D* **102** (2020) 054516 [[1910.08516](#)].
- [31] A. Vilenkin, *Equilibrium parity violating current in a magnetic field*, *Phys. Rev. D* **22** (1980) 3080.
- [32] N. Yamamoto, *Generalized Bloch theorem and chiral transport phenomena*, *Phys. Rev. D* **92** (2015) 085011 [[1502.01547](#)].
- [33] B.B. Brandt, G. Endrődi, E. Garnacho-Velasco and G. Markó, *The chiral separation effect from lattice QCD at the physical point*, *JHEP* **02** (2024) 142 [[2312.02945](#)].
- [34] D.T. Son and A.R. Zhitnitsky, *Quantum anomalies in dense matter*, *Phys. Rev. D* **70** (2004) 074018 [[hep-ph/0405216](#)].

- [35] M.A. Metlitski and A.R. Zhitnitsky, *Anomalous axion interactions and topological currents in dense matter*, *Phys. Rev. D* **72** (2005) 045011 [[hep-ph/0505072](#)].
- [36] K. Fukushima, D.E. Kharzeev and H.J. Warringa, *Real-time dynamics of the Chiral Magnetic Effect*, *Phys. Rev. Lett.* **104** (2010) 212001 [[1002.2495](#)].
- [37] G. Bali and G. Endrődi, *Hadronic vacuum polarization and muon $g-2$ from magnetic susceptibilities on the lattice*, *Phys. Rev. D* **92** (2015) 054506 [[1506.08638](#)].
- [38] G.S. Bali, G. Endrődi and S. Piemonte, *Magnetic susceptibility of QCD matter and its decomposition from the lattice*, *JHEP* **07** (2020) 183 [[2004.08778](#)].
- [39] P.V. Buividovich, D. Smith and L. von Smekal, *Static magnetic susceptibility in finite-density $SU(2)$ lattice gauge theory*, *Eur. Phys. J. A* **57** (2021) 293 [[2104.10012](#)].
- [40] X.-l. Sheng, D.H. Rischke, D. Vasak and Q. Wang, *Wigner functions for fermions in strong magnetic fields*, *Eur. Phys. J. A* **54** (2018) 21 [[1707.01388](#)].
- [41] J.S. Schwinger, *On gauge invariance and vacuum polarization*, *Phys. Rev.* **82** (1951) 664.
- [42] I.A. Shovkovy, *Magnetic Catalysis: A Review*, *Lect. Notes Phys.* **871** (2013) 13 [[1207.5081](#)].
- [43] C. Itzykson and J.B. Zuber, *Quantum Field Theory*, International Series In Pure and Applied Physics, McGraw-Hill, New York (1980).
- [44] D. Hou, H. Liu and H.-c. Ren, *Some Field Theoretic Issues Regarding the Chiral Magnetic Effect*, *JHEP* **05** (2011) 046 [[1103.2035](#)].
- [45] D. Bohm, *Note on a theorem of Bloch concerning possible causes of superconductivity*, *Phys. Rev.* **75** (1949) 502.
- [46] S. Borsányi, G. Endrődi, Z. Fodor, A. Jakovác, S.D. Katz, S. Krieg et al., *The QCD equation of state with dynamical quarks*, *JHEP* **11** (2010) 077 [[1007.2580](#)].
- [47] M. Constantinou, M. Hadjiantonis, H. Panagopoulos and G. Spanoudes, *Singlet versus nonsinglet perturbative renormalization of fermion bilinears*, *Phys. Rev. D* **94** (2016) 114513 [[1610.06744](#)].
- [48] RQCD collaboration, *Masses and decay constants of the η and η' mesons from lattice QCD*, *JHEP* **08** (2021) 137 [[2106.05398](#)].
- [49] G.S. Bali, F. Bruckmann, G. Endrődi, Z. Fodor, S.D. Katz, S. Krieg et al., *The QCD phase diagram for external magnetic fields*, *JHEP* **02** (2012) 044 [[1111.4956](#)].
- [50] H.S. Sharatchandra, H.J. Thun and P. Weisz, *Susskind Fermions on a Euclidean Lattice*, *Nucl. Phys. B* **192** (1981) 205.
- [51] S. Dürr, *Taste-split staggered actions: eigenvalues, chiralities and Symanzik improvement*, *Phys. Rev. D* **87** (2013) 114501 [[1302.0773](#)].
- [52] P. Hasenfratz and F. Karsch, *Chemical Potential on the Lattice*, *Phys. Lett. B* **125** (1983) 308.
- [53] V.V. Braguta, V.A. Goy, E.M. Ilgenfritz, A.Y. Kotov, A.V. Molochkov, M. Müller-Preussker et al., *Two-Color QCD with Non-zero Chiral Chemical Potential*, *JHEP* **06** (2015) 094 [[1503.06670](#)].
- [54] N.Y. Astrakhantsev, V.V. Braguta, A.Y. Kotov, D.D. Kuznedev and A.A. Nikolaev, *Lattice study of QCD at finite chiral density: topology and confinement*, *Eur. Phys. J. A* **57** (2021) 15 [[1902.09325](#)].

- [55] V.V. Braguta, E.M. Ilgenfritz, A.Y. Kotov, B. Petersson and S.A. Skinderev, *Study of QCD Phase Diagram with Non-Zero Chiral Chemical Potential*, *Phys. Rev. D* **93** (2016) 034509 [[1512.05873](#)].
- [56] L.H. Karsten and J. Smit, *Lattice Fermions: Species Doubling, Chiral Invariance, and the Triangle Anomaly*, *Nucl. Phys. B* **183** (1981) 103.
- [57] G.S. Bali, B.B. Brandt, G. Endrődi and B. Gläfle, *Meson masses in electromagnetic fields with Wilson fermions*, *Phys. Rev. D* **97** (2018) 034505 [[1707.05600](#)].
- [58] G.S. Bali, B.B. Brandt, G. Endrődi and B. Gläfle, *Weak decay of magnetized pions*, *Phys. Rev. Lett.* **121** (2018) 072001 [[1805.10971](#)].
- [59] G.S. Bali, F. Bruckmann, G. Endrődi, Z. Fodor, S.D. Katz and A. Schäfer, *QCD quark condensate in external magnetic fields*, *Phys. Rev. D* **86** (2012) 071502 [[1206.4205](#)].
- [60] G. Endrődi, *Multidimensional spline integration of scattered data*, *Comput. Phys. Commun.* **182** (2011) 1307 [[1010.2952](#)].
- [61] B.B. Brandt, F. Cuteri, G. Endrődi, G. Markó, L. Sandbote and A.D.M. Valois, *Thermal QCD in a non-uniform magnetic background*, *JHEP* **11** (2023) 229 [[2305.19029](#)].
- [62] D.R. Hofstadter, *Energy levels and wave functions of Bloch electrons in rational and irrational magnetic fields*, *Phys. Rev. B* **14** (1976) 2239.
- [63] G. Endrődi, *QCD in magnetic fields: from Hofstadter's butterfly to the phase diagram*, *PoS LATTICE2014* (2014) 018 [[1410.8028](#)].
- [64] F. Bruckmann, G. Endrődi, M. Giordano, S.D. Katz, T.G. Kovács, F. Pittler et al., *Landau levels in QCD*, *Phys. Rev. D* **96** (2017) 074506 [[1705.10210](#)].
- [65] R. Bignell, W. Kamleh and D. Leinweber, *Pion magnetic polarisability using the background field method*, *Phys. Lett. B* **811** (2020) 135853 [[2005.10453](#)].